ADVANCED FUNCTIONAL MATERIALS
www.afm-journal.de

A Top Coat with Solvent Annealing Enables Perpendicular Orientation of Sub-10 nm Microdomains in Si-Containing Block Copolymer Thin Films

*Eunjin Kim, Wonjung Kim, Kwang Hee Lee, Caroline A. Ross, and Jeong Gon Son**

Achieving sub-10 nm high-aspect-ratio patterns from diblock copolymer self-assembly requires both a high interaction parameter (χ, which is determined by the incompatibility between the two blocks) and a perpendicular orientation of microdomains. However, these two conditions are extremely difficult to achieve simultaneously because the blocks in a high-χ copolymer typically have very different surface energies, favoring in-plane microdomain orientations. A fully perpendicular orientation of a high-χ block copolymer, poly(styrene-*block*-dimethylsiloxane) (PS-*b*-PDMS) is realized here using partially hydrolyzed polyvinyl alcohol (PVA) top coats with a solvent annealing process, despite the large surface energy differences between PS and PDMS. The PVA top coat on the block copolymer films under a solvent vapor atmosphere significantly reduces the interfacial energy difference between two blocks at the top surface and provides sufficient solvent concentration gradient in the through-thickness direction and appropriate solvent evaporation rates within the film to promote a perpendicular microdomain orientation. The effects of interfacial energy differences and the swellability of PVA top coats controlled by the degree of hydrolysis on the orientation of microdomains are examined. The thickness of the BCP film and top coats also affects the orientation of the BCP film.

1. Introduction

The self-assembly of block copolymers (BCPs), which spontaneously form nanosized microdomains with dimensions from a few nm to several hundred nm, have been investigated for many potential applications including next generation lithography,[1–4] nanoporous membranes[5,6] and photonic crystals.[7] For smaller sized patterns beyond the limitations of conventional lithographic tools,[8] a high interaction parameter (χ) is required to ensure a driving force for microphase separation even at the sub-10 nm scale, and high etch selectivity is required to enable pattern transfer to other materials. A perpendicular orientation of BCP cylindrical or lamellar microdomains facilitates pattern transfer and the formation of porous films.

In thin films of BCPs, a difference in surface energies between the blocks promotes microdomain orientation parallel to the surface,[9] and there has been considerable work done on instead producing a perpendicular microdomain orientation in a thin film.[10–14] Equalization of the surface energies of the blocks during thermal annealing promotes a perpendicular microdomain orientation in a thin film at the air surface, and equalization of the interface energies promotes a perpendicular orientation at the substrate interface. In the case of polystyrene-*block*-poly(methyl methacrylate) (PS-*b*-PMMA), the blocks have similar surface energies, and substrate neutrality can be achieved by coating the surface with a random copolymer brush[12] or a self-assembled monolayer (SAM).[13] Neutrality of the top surface of PS-*b*-PMMA films has also been obtained at specific temperature (≈250 °C) for the identical surface energy[15] or by the addition of surfactants.[14] However, this neutralizing approach is limited to a narrow range of surface energy differences[16] and the perpendicular domain orientation is dependent on the film thickness.[17–20] Thicker films often form a mixed orientation where parallel orientations occur at the top and perpendicular orientations at the bottom surface,[12,13,20,21] unless surface neutrality and substrate neutrality are simultaneously satisfied. Furthermore, PS-*b*-PMMA does not exhibit microphase separation at the sub-20 nm scale because of its relatively low χ parameter ($\chi_{PS\text{-}PMMA} \approx 0.03$ at 25 °C).[22] Other BCPs, such as polystyrene-*block*-poly(2-vinyl pyridine), have shown greater difficulty in forming a fully perpendicular orientation using the neutral surface/interface

E. Kim, Dr. J. G. Son
Photo-Electronic Hybrids Research Center
Korea Institute of Science and Technology (KIST)
Seoul 136–791, Korea
E-mail: jgson@kist.re.kr
E. Kim, Prof. K. H. Lee
Department of Polymer Science and Engineering
Inha University
Incheon 402–751, Korea
Prof. W. Kim
Department of Mechanical Engineering
Sogang University
Seoul 121–742, Korea
Prof. C. A. Ross
Department of Materials Science and Engineering
Massachusetts Institute of Technology
Cambridge, MA 02139, USA

DOI: 10.1002/adfm.201401678

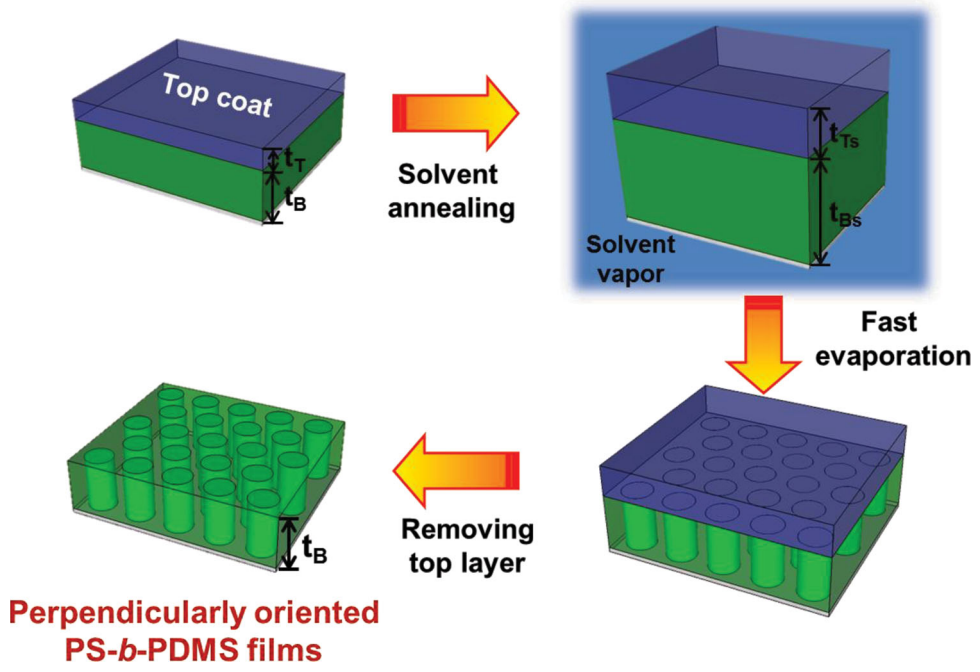

Figure 1. Schematics of the solvent annealing process of block copolymer thin films with a top coat layer to produce a perpendicular orientation of microdomains. Top coats were carefully chosen for solvent permeability during solvent annealing and were simply removed with a non-solvent for both blocks of the BCP.

approach with a thermal annealing process.[23] Recently, perpendicular orientation was demonstrated using a removable neutral top coat of a polarity-switching terpolymer[24–26] which produced a neutral top surface ($\Delta\gamma_{Top} = 0$). However, the perpendicular orientation was only obtained at certain film thicknesses for modest non-zero $\Delta\gamma_{Top} < 0.5$ mN m^{-1}, and the process was challenging for high-χ BCPs.

Solvent annealing is another promising approach to obtain perpendicular orientation.[5,6,27–30] Solvent molecules swell the BCP films and increase the mobility of BCP chains. Then, during the solvent evaporation process, the through-thickness solvent concentration gradient can kinetically generate a perpendicular orientation of the BCP microdomains,[27] despite the relatively high surface or interfacial energy difference. However, the vapor pressure condition and deswelling process need to be closely controlled, and perpendicular orientations were only demonstrated in films that exceeded several hundred nm thick.[6,29]

We have previously investigated sub-10 nm diameter in-plane microdomains from a cylindrical-morphology polystyrene-*block*-polydimethylsiloxane (PS-*b*-PDMS)[31–34] BCP, which has a high χ parameter recently calculated as $\chi_{PS\text{-}PDMS} \approx 0.14$ at 25 °C.[22] This BCP has a high etch selectivity between the silicon-containing PDMS and the PS in an oxygen plasma. However, it has been difficult to produce perpendicularly oriented PS-*b*-PDMS microdomains because of the large difference in surface energy between PS ($\gamma_{PS} \approx 40.7$ mN m^{-1}) and PDMS ($\gamma_{PDMS} \approx 20.4$ mN m^{-1}).[35] Our previous study on films a few 100 nm thick[36] using slow solvent evaporation produced a perpendicular orientation of PS-*b*-PDMS throughout the film thickness except at the top surface where a few layers of in-plane oriented cylindrical microdomains formed.

Here, we introduce a process that combines a top coat layer with a solvent anneal to achieve fully perpendicular orientation of microdomains in a high-χ block copolymer. This process simultaneously employs top surface neutrality and a sufficient film thickness for the control of the solvent concentration gradient and evaporation rate. A through-thickness perpendicular orientation of sub-10 nm diameter PS-*b*-PDMS block copolymer microdomains was formed from 25–700 nm thick films using partially hydrolyzed polyvinyl alcohol (PVA) as a top coat layer and solvent annealing in acetone. The effects of the BCP film thickness, top layer thickness, interfacial energy differences and swelling of the top layer on the microdomain orientations were demonstrated. This approach can be used to make highly regular porous membranes with sub-10 nm pores through the PVA sacrificial layer and the selective swelling of the PDMS domains.

2. Results and Discussion

The top coat/solvent annealing system is schematically shown in **Figure 1**. The top coat is formed by spin-coating on the BCP film. During the solvent annealing process, the top coat should be permeable and swellable by the solvent molecules and maintain a smooth interface with the BCP film. A straightforward removal process is also required after the BCP annealing is complete. A partially hydrolyzed PVA film was selected as a top coat for PS-*b*-PDMS because it can be deposited by spin-coating and removed by rinsing with water or methanol without damaging the underlying BCP film, and it undergoes moderate swelling but no dewetting under an acetone vapor atmosphere. Furthermore, differently hydrolyzed PVAs provide an additional

Table 1. Surface and calculated interfacial tensions of PS and PDMS with air; a Si substrate; and 40%, 80%, and 89% hydrolyzed PVA, both for the melt and for the swollen state.

$\gamma_{PS\text{-}Top}$	PS-air	PS-Si wafer	PS-PVA40	PS-PVA80	PS-PVA89
Melt	40.7 mN m^{-1}	18.7 mN m^{-1}	4.67 mN m^{-1}	7.10 mN m^{-1}	7.71 mN m^{-1}
Swollen state	32.1 mN m^{-1}	19.0 mN m^{-1}	1.28 mN m^{-1}	4.25 mN m^{-1}	8.70 mN m^{-1}
$\gamma_{PDMS\text{-}Top}$	PDMS-air	PDMS-Si wafer	PDMS-PVA40	PDMS-PVA80	PDMS-PVA89
Melt	20.4 mN m^{-1}	30.2 mN m^{-1}	14.7 mN m^{-1}	19.3 mN m^{-1}	20.3 mN m^{-1}
Swollen state	20.9 mN m^{-1}	27.7 mN m^{-1}	4.73 mN m^{-1}	11.0 mN m^{-1}	17.7 mN m^{-1}

opportunity to control the interfacial energy differences and swellability according to the degree of hydrolysis from polyvinyl acetate to PVA. 40%, 80% and 89% hydrolyzed PVA was used for the top layers in this study. The surface and interfacial energies of PS and PDMS with various top coats and on a Si substrate both in the molten state and in a swollen state[37] were calculated using Wu's method[35] and surface tension changes of semi-dilute polymer solutions in θ-solvent conditions.[37] These results are presented in **Table 1**[35,38,39] and their swelling ratios in acetone vapor were measured and are shown in **Table 2.** Less hydrolyzed PVA, such as the 40% hydrolyzed PVA (PVA40), shows lower interfacial energy with PS and PDMS and higher swelling in acetone vapor than highly hydrolyzed PVA. This is because the Hildebrand solubility parameter of polyvinyl acetate (≈19.6 MPa$^{1/2}$) is much closer to that of PS (≈17.5 MPa$^{1/2}$), PDMS (≈15.0 MPa$^{1/2}$) and acetone (≈20.3 MPa$^{1/2}$) than that of the fully hydrolyzed PVA (≈25.8 MPa$^{1/2}$).[40] The solvent annealing process additionally enabled a reduction in the interfacial energy differences of the swollen polymers compared with that of the melt phase, as shown in Table 1.[41]

An ideal top coat should reduce the difference in interfacial energies between the BCP domains and provide a sufficient pathway for the solvent molecules during the swelling and deswelling processes. Among the three top coats investigated, PVA40 leads to the smallest difference of interfacial energies between PS and PDMS ($\Delta\gamma_{PVA40\text{-}Swollen} \approx 3.45$ mN m^{-1}), swells even more than PS-*b*-PDMS films under acetone vapor and thus may be the best top coat to obtain a perpendicular orientation of PS-*b*-PDMS films.

Figure 2 shows the results of annealing the 16 kg/mol cylindrical PS-*b*-PDMS ($f_{PDMS} \approx 0.31$, PDI ≈ 1.08) films with and without PVA40 top coats. BCP films were produced on as-received Si wafers from a 0.5–7 wt% solution in cyclohexane. For the introduction of the ≈200 nm top coats, 4 wt% PVA40 solution in methanol was spin-coated at 8000 rpm on the BCP films. After annealing thermally or in a solvent vapor, the PVA40 top layers were removed by a thorough rinse with methanol. Images of the PDMS microdomains were obtained by a 50 W CF_4 reactive ion etching (RIE) treatment for 3 s to remove any PDMS wetting layer at the top surface, followed by a 90 W O_2 RIE for 20 s to etch the PS microdomains selectively, leaving the oxidized PDMS microdomains.

Firstly, as a reference, BCP films with a thickness of 200 nm without top coats were thermally annealed at 170 °C for 24 h in a vacuum atmosphere. The films showed in-plane PDMS cylinders with a 11.7 nm width and a 19.4 nm period at the top surface, with the in-plane orientation driven by the surface energy difference between PS and PDMS (Figure 2a). BCP films (≈200 nm) with PVA40 top coats also resulted in a parallel orientation of cylinders throughout the thickness under thermal annealing (Figure 2b). This is because even though the interfacial energy difference between PS-PVA40 (≈4.67 mN m^{-1}) and PDMS-PVA40 (≈14.7 mN m^{-1}) was smaller than the interfacial energy difference between PS-air and PDMS-air, the surface energy difference was still sufficient to produce an in-plane microdomain orientation.

In comparison, films were also solvent annealed in acetone vapor and showed dramatically different alignment of the BCP microdomains. Solvent annealing of the BCP films was performed for 30 min in a PTFE chamber under a controlled acetone vapor pressure P where $P/P_s \approx 0.95$ and P_s is the saturated vapor pressure of acetone. System details are described in Figure S1 (Supporting Information). The samples were quickly removed from the chamber to obtain rapid evaporation of solvent from the film. Without top coats, as observed in Figure 2c,d, in-plane cylinders of BCP microdomains were observed at the top surface, but perpendicularly oriented cylinders were observed in the bulk of the films and at the bottom interface, similar to our previous study.[36] These mixed morphologies were a result of the competition between the solvent evaporation process causing perpendicular microdomain orientation in the bulk of the film, and the high surface energy difference between PS and PDMS leading to in-plane orientation near the surface. The solvent annealing process could overcome the interfacial energy differences at the bottom interface with the Si wafer ($\Delta\gamma_{Bottom\text{-}Swollen} \approx 8.7$ mN m^{-1}) to give perpendicular alignment at the substrate, but not at the air interface ($\Delta\gamma_{Top\text{-}Swollen} \approx 11.2$ mN m^{-1}).

In the case of top coats with solvent annealing, the films showed fully perpendicularly oriented cylinder arrays with 18.2 nm period and cylinder diameter of 9.7 nm extending through the film thickness as shown in the in-plane SEM image (Figure 2e) and cross-section image in 70 nm (Figure 2f) and 700 nm

Table 2. Swelling ratios of the PS-*b*-PDMS, PS and PDMS films and variously hydrolyzed PVA films under $P/P_s = 0.95$ of acetone vapor at 22 °C.

	PS-b-PDMS	PS	PDMS	PVA, 40% hydrolysis	PVA, 80% hydrolysis	PVA, 89% hydrolysis
Acetone ($P/P_s \approx 0.95$)	1.32	1.37	1.18	1.61	1.22	1.01

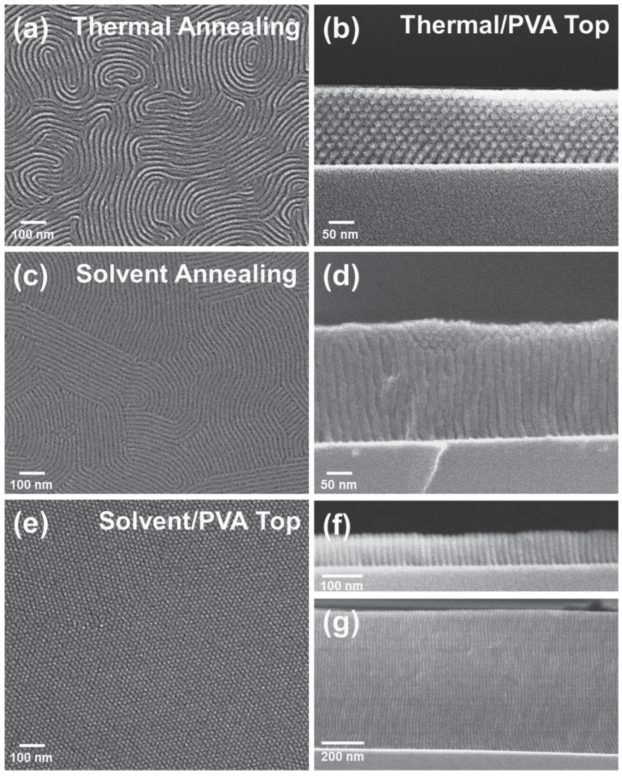

Figure 2. SEM images of differently treated PS-*b*-PDMS films after O_2 plasma treatment for image contrast. a) In-plane image of 250 nm thick BCP films without a top coat under thermal annealing at 170 °C for 24 h and b) cross-sectioned image of a thermally annealed 250 nm film with 40% hydrolyzed PVA top coat. c) In-plane and d) cross-sectional images of solvent annealed 300 nm thick films without a top coat using an acetone vapor ($P/P_s \approx 0.95$) for 30 min. e) In-plane and f) cross-sectional image of 70 nm thick BCP films with a 40% hydrolyzed PVA top coat after solvent annealing. g) BCP films with a 700 nm thickness with top coat and solvent annealing. The thickness of the top coat was 200 nm.

(Figure 2g) films. This perpendicular orientation was typically obtained from 25–700 nm thick films and it did not cause any roughening of the top surface. Because the top coats could efficiently reduce the top surface energy difference ($\Delta\gamma_{\text{Top-Swollen}}$) from ≈11.2 mN m^{-1} to ≈3.45 mN m^{-1}, a perpendicular orientation could be formed all the way through the films in the solvent annealing system. Based on these results, we conclude that the solvent annealing process can overcome a substantial high surface/interfacial energy difference and enlarge the neutral zone at which perpendicular orientation of BCP films can occur.

To understand the effects of the surface energy and swelling properties of the top layer on the microdomain morphology, variously hydrolyzed PVAs were introduced as top coats while the solvent annealing conditions were unchanged. **Figure 3**a–c shows top surface morphologies of 150 nm thick BCP films with 40%, 80% (PVA80) and 89% (PVA89) hydrolyzed PVA top coats and a thickness of 200 nm. While the PVA40 top coats produed a fully perpendicular orientation (Figure 3a), the PVA80 top coats produced regions of parallel and perpendicular oriented cylinders co-existing at the top surface, as shown in Figure 3b, attributed to a higher interfacial energy difference compared with that of PVA40. The swellability of PVA80 was comparable with the PS-*b*-PDMS films under an acetone vapor. However, the PVA89 treated BCP films (Figure 3c) showed poorly ordered cylinders because the PVA89 top coats had almost no swelling in acetone vapor, creating a barrier which hindered annealing of the BCP films and preventing BCP swelling.

The block copolymer film thickness played an important role in determining the orientation of the microdomains. To illustrate this more dramatically, we used PVA80, in which a mixed surface orientation was present when the BCP thickness was 150 nm. Figure 3b,d,e shows top surface orientations of b) 150 nm, d) 50 nm and e) 300 nm thick BCP films with 200 nm PVA80 top coats after solvent annealing with acetone. As the films become thinner, effects of the interfaces on the microdomain orientation become proportionately more important. The

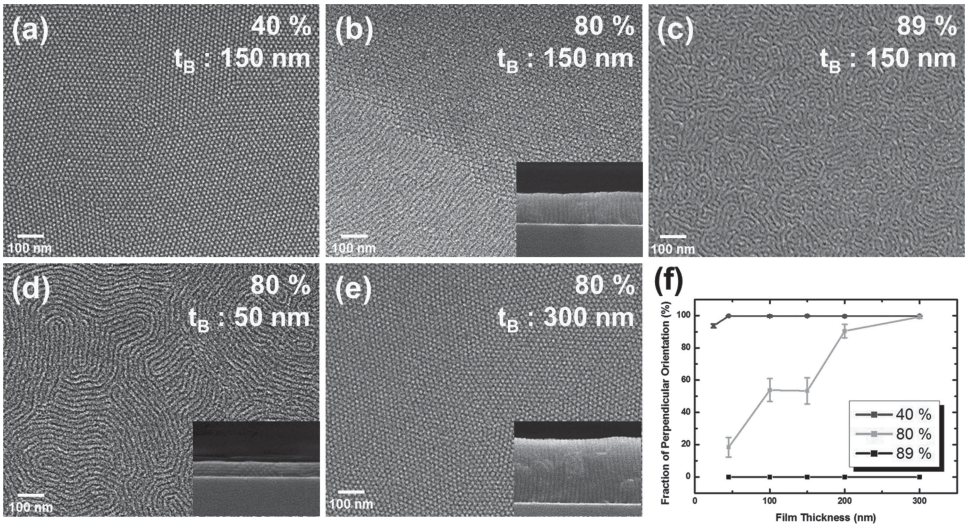

Figure 3. A sampling of morphologies observed for different top coats with differing film thicknesses using solvent annealing with acetone. a–c) PS-*b*-PDMS films, 150 nm thick, with a 200 nm thickness of a) 40%, b) 80% and c) 89% hydrolyzed PVA top coat. d–f) 80% hydrolyzed PVA top coat on the d) 50 nm and e) 300 nm thick PS-*b*-PDMS films. f) The fraction of perpendicular orientation of cylinders as a function of BCP film thickness and degree of hydrolysis of the PVA top coat.

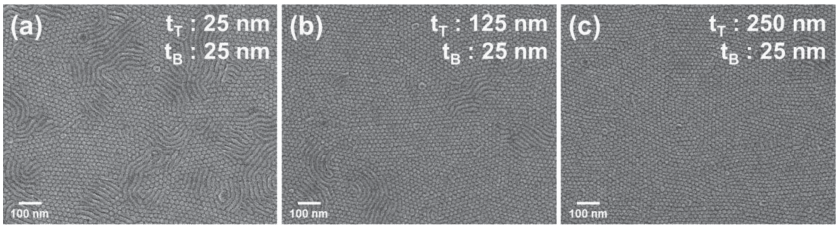

Figure 4. The orientation changes of 25 nm thick PS-*b*-PDMS thin films according to various thicknesses of PVA40 top coats from a) 25 nm, b) 125 nm to c) 250 nm.

50 nm thick BCP films showed mostly in-plane cylinders with a small amount of perpendicular orientation, but the 300 nm films had an almost complete perpendicular orientation. Image analysis of at least 10 images per sample was performed to obtain the area fraction of perpendicular orientation at the top surface vs. the degree of hydrolysis and BCP film thickness in Figure 3f. PVA40 produced a perpendicular orientation regardless of film thickness, and PVA89 rarely formed a perpendicular orientation at any thickness, while PVA80 showed a gradual increase in perpendicular orientation as the thickness increased.

The thickness of the top coat is also an important factor determining the microdomain orientation as shown in **Figure 4** for 25 nm thick BCP films with 25, 125 and 250 nm thick PVA40 top coats. As the top coat became thicker the orientation at the top surface of the BCP changed from mixed to perpendicular. These results are attributed to the effect of the top coat on the solvent concentration profile during evaporation.

Phillip et al.[42] theoretically deduced that the microdomain orientation of BCP films depends on the gradient of the solvent concentration in the swollen polymer film during the drying process. Paradiso et al.[43] presented a computational analysis suggesting that a perpendicular orientation cannot form during an extremely fast evaporation process. Although these studies focused on solvent annealing for a BCP film with a thickness on the order of 100 μm, our experimental results can be explained on the basis of the same theoretical framework.

We begin with the consideration of a polymer film containing a homogeneously distributed solvent without a top coat. The polymer film is placed on an impermeable substrate and exposed to an atmosphere where the solvent concentration is negligible. We assume that the solvent is allowed to evaporate only through the top surface of the film and that the film thickness l_0 is not changed during the evaporation. The solvent concentration of this polymer film is described by the one-dimensional Fick's law:

$$\frac{\partial \phi}{\partial t} = D\frac{\partial^2 \phi}{\partial z^2} \tag{1}$$

where φ is the solvent concentration, D is the diffusion coefficient of solvent in the film, z is the distance from the top surface of the film, and t is the evaporation time. This governing equation has the initial and boundary conditions:

$$\phi = \phi_0, 0 < z < l_0, t = 0 \tag{2}$$

$$\frac{\partial \phi}{\partial z} = 0, z = l_0, > 0 \tag{3}$$

$$D\frac{\partial \phi}{\partial z} = \frac{k}{H}\phi, z = 0, t > 0 \tag{4}$$

where ϕ_0 is the initial solvent concentration, k is the mass transfer coefficient at the air-film interface and H is the partition coefficient, which is the ratio of the solvent concentration in the film to that at equilibrium in the vapor. Using the parameters $D \approx 10^{-11}$ m^2 s^{-1}, $H \approx 800$, and $k \approx 0.01$ m s^{-1} for typical experimental settings for film evaporation,[42] Equation (1) can be numerically solved with boundary and initial conditions in Equations (2)–(4).

Figure 5a presents the solvent concentration with respect to z and t for different film thicknesses of 50 nm, 150 nm, 300 nm

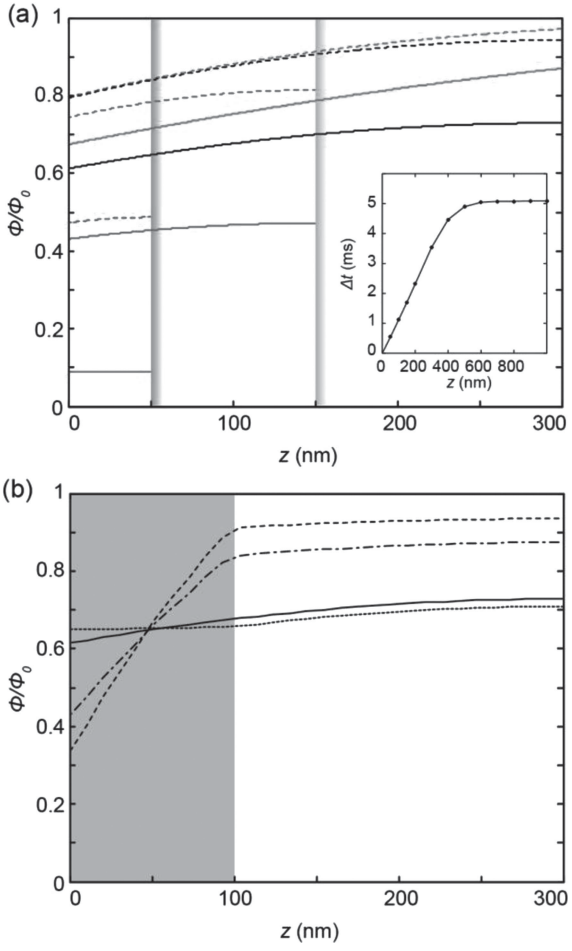

Figure 5. Solvent concentration profiles for BCP films on an impermeable substrate. a) The upper surface of BCP films is bare. The green, black, blue, and red lines correspond to thicknesses of ∞, 300 nm, 150 nm, and 50 nm, respectively. The dashed and solid lines correspond to the concentration profiles at 0.003 s and 0.01 s, respectively. The parameters are given by $D = 10^{-11}$ m^2 s^{-1}, $H = 800$, and $k = 0.01$ m s^{-1}. Inset: the time duration for the change of the solvent concentration from 0.8 to 0.7 at the top surface. b) BCP films with a thickness of 200 nm are covered with a top coat with a thickness of 100 nm. Profiles correspond to 0.01 s. The dashed, dash-dotted, solid, and dotted lines denote the diffusivity of the top coat of 0.05 D, 0.1D, D, and 10D, respectively.

and a semi-infinite thick film. The concentration profiles at an early stage of evaporation, 0.003 s and 0.01 s, are shown because the order-disorder transition of conventional BCPs occurred at a solvent concentration of 0.8–0.7 of its initial concentration according to experimental[44] and calculated results.[42] The results indicate that films with a thickness of 300 nm produced gradients of the solvent concentration similar to those of a semi-infinite film, whereas thin films with a thickness of 50 nm yield a smaller concentration gradient and a faster evaporation rate compared with thicker films, impeding the formation of the perpendicular orientation. Because the formation of the ordered phase at the surface takes place over a certain time interval,[42] rapid evaporation cannot yield fully perpendicular cylinders.[43]

To describe the top coat system, we now insert a 100 nm thick upper layer which has a different diffusion coefficient (10D, 0.1D, 0.05D) above the 200 nm block copolymer layer (diffusion coefficient D) and illustrate the solvent concentration profiles in Figure 5b. A highly diffusive top coat does not make much difference to the solvent concentration gradient compared with that of a 300 nm monolithic film. However, a less diffusive top coat restricts the evaporation of solvent and a significant solvent gradient exists in the top coat, yielding a smaller concentration gradient in the underlying BCP film. The results indicate that a top coat with a similar diffusion coefficient to that of the BCP effectively increases the BCP film thickness to produce a concentration gradient leading to perpendicular orientation, whereas a less diffusive top coat provides a barrier against solvent evaporation and reduces the concentration gradient in the BCP film.

The Biot number, $Bi = kl_0/(DH)$, which describes the ratio of the mass transfer resistances inside and at the surface of the film, critically determines the gradient of solvent concentrations and evaporation rates. Assuming that the solvent annealed BCP/top coat bilayer film with a thickness of 300 nm can marginally achieve a perpendicular orientation, as implied by our experimental results, we deduce the critical Biot number, $Bi_c \approx 0.4$, below which the perpendicular orientation cannot be achieved. Accordingly, for a film with $Bi < 0.4$, top coating provides a novel strategy aiming to produce a sharp gradient of the solvent concentration and sufficiently controlled evaporation rates.

The PVA layer can also be used as an underlayer or as a sandwich structure with the BCP film to provide control over the bottom interface of the BCP. Samples of 250 nm PVA80 were spin-coated from aqueous solution, then 250 nm BCP films, then an optional 350 nm PVA40 film to form a sandwich structure. The PVA80 underlayer can also serve as a sacrificial layer for floating the BCP film on the water surface, enabling the bottom surface of the BCP to be easily imaged. Cross-sectional images were also obtained, but the PVA layers were significantly damaged by electron beam irradiation and disappeared during scanning electron microscopy (SEM) imaging. **Figure 6**a,b shows the orientation of a BCP film with a PVA80 underlayer that exhibited a perpendicular orientation at the bottom interface in contact with the PVA80 and in the bulk of the film but had a parallel orientation at the air surface. However, in the case of a PVA80/BCP/PVA40 sandwich structure, a perpendicular orientation was observed all the way through the film, as in Figure 6c,d.

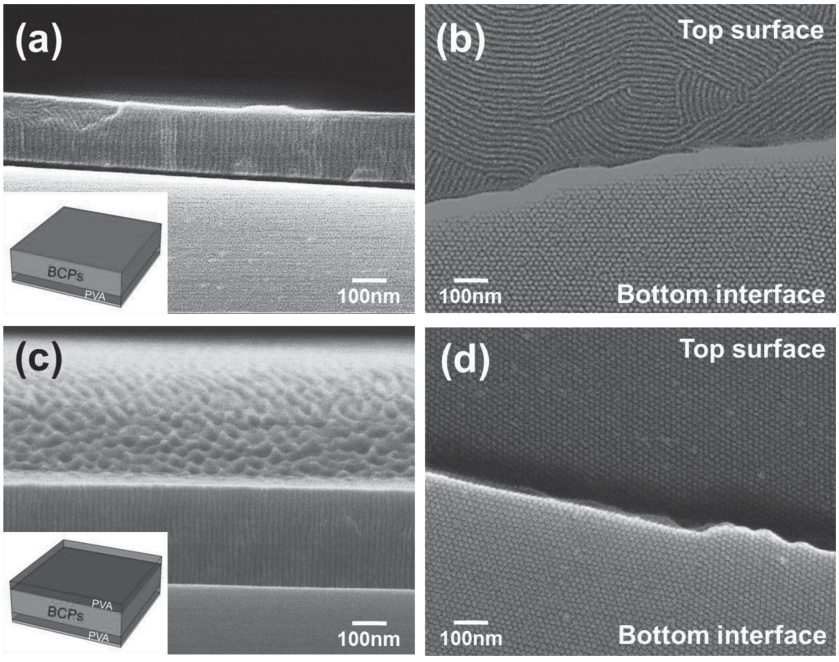

Figure 6. PS-*b*-PDMS films with a,b) PVA80 underlayer and c,d) a PVA80/BCP/PVA40 sandwich structure for the control of orientation. a) Cross-sectional image of a 250 nm thick BCP film on a 250 nm PVA80 underlayer and b) in-plane image of flipped BCP films, obtained after dissolving the PVA80 underlayer, to co-observe the orientations at the top surface and bottom interface. c) Cross-sectional SEM image and d) in-plane image of a flipped sample of PVA80/BCP/PVA40 (350 nm/250 nm/250 nm) sandwich structure.

The easy removal of the sandwich structure in water facilitates its transfer to other substrates. If sub-10 nm hole structures are produced from BCP films with a perpendicular microdomain orientation, this method can be directly used to form a nanoporous membrane with a highly regular pore size distribution. Therefore, a selective swelling method[6] was introduced to PS-*b*-PDMS films to make porous structures. Immersing the films into perfluorooctane at 50 °C for 30 min, as a selective solvent for PDMS, the PDMS cylindrical domains were selectively swollen and solvent removal created sub-10 nm pores with their inner surfaces covered with PDMS, as illustrated in **Figure 7**. This approach can be used for PS-*b*-PDMS films to make sub-10 nm highly regular and highly hydrophobic porous membranes.

3. Conclusion

Fully perpendicular arrays of sub-10 nm diameter high-aspect ratio microdomains can be produced in PS-*b*-PDMS films using partially hydrolyzed PVA top coats and a solvent annealing process, despite large surface energy differences between PS and

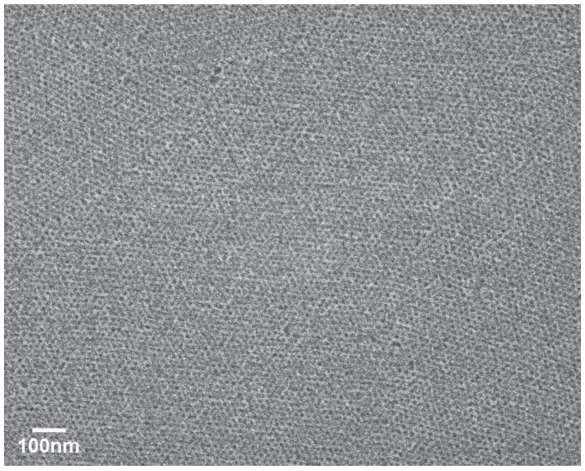

Figure 7. SEM image of the nanoporous structures of perpendicularly oriented cylindrical microdomains of PS-*b*-PDMS thin films. The films were immersed in perfluorooctane at 50 °C for 30 min to selectively swell the PDMS domains and form cylindrical pores in the films.

PDMS. The PVA top coats not only efficiently reduce the interfacial energy between PS and PDMS at the top surface but also control the through-thickness solvent concentration gradient and the solvent evaporation rates. Differently hydrolyzed PVA films are effective top coats for PS-*b*-PDMS because the interfacial energy can be controlled easily according to the degree of hydrolysis and the films can be removed in water. The thickness of the BCP film and top coat were important factors that affected the orientation of the BCP film. Using this approach, sub-10 nm period high-aspect-ratio patterns can be obtained from a high χ block copolymer, which is useful in next generation nanolithography or as nanoporous membranes.

4. Experimental Section

BCPs and Top Coat Layer Preparation: PS-*b*-PDMS (Mw ≈ 16 kg mol^{-1}, 11-*b*-5 kg mol^{-1}, PDI ≈ 1.08, purchased from Polymer Source, Inc., Quebec, Canada) solution in cyclohexane was spin-coated on as-received Si substrates. By varying the concentration of solution from 1 to 5 wt%, the thicknesses of the BCPs films was controlled from 50 nm to 300 nm. The film thickness was measured using Filmetrics F20. 80% hydrolyzed PVA (Mw ≈ 9–10 kg mol^{-1}) and 89% hydrolyzed PVA (Mw ≈ 13–20 kg mol^{-1}) were purchased from Sigma Aldrich, Inc., and 40% hydrolyzed PVA (Mw ≈ 72 kg mol^{-1}) was purchased from Polyscience, Inc. The PVA solutions dissolved in deionized water or methanol were spin-coated directly onto the BCP films. By varying the concentration of solution from 2–10 wt%, the thicknesses of the PVA film was controlled from 50 nm to 300 nm. The films were dried in a vacuum condition to remove residual solvent.

Solvent Annealing and Pattern Formation: Solvent annealing was carried out using a mass flow controlled saturated acetone vapor with nitrogen in a Teflon chamber for 30 min. The annealed films were quickly moved out of the chamber to induce fast solvent evaporation along the film thickness direction. After solvent annealing, the top PVA film was simply removed by water or methanol rinsing, and the BCPs films were dried with nitrogen gas. The BCPs film was optionally treated with CF_4 RIE (5 s, 50 W) to etch the PDMS surface layer in samples with parallel microdomain orientation, and O_2 RIE (30 s or more, 90 W) to selectively remove the PS domains and produce high-aspect-ratio perpendicular oriented nanostructures. For the nanoporous structures, the films were immersed into a perfluorooctane solution (98%, Sigma Aldrich, Inc.) at 50 °C for 30 min.

Pattern Characterization: To observe the morphology of the BCPs at the BCP/PVA underlayer interface, the BCP/PVA film was solvent annealed in the same fashion as the BCPs film, with the top layer of PVA. The films were partially immersed in DI water to dissolve the PVA sacrificial layer, and the released polymer film was flipped over to expose the bottom interface of the film. Samples for the cross sectional morphology of BCPs were fully quenched in liquid nitrogen for 1 min and then notched. The morphology of the block copolymer patterns was observed by a field emission-scanning electron microscope (FE-SEM, JEOL) operated at 10 kV. The samples for FE-SEM were coated with a thin Pt film to avoid charging effects.

Supporting Information

Supporting Information is available from the Wiley Online Library or from the author.

Acknowledgements

The authors gratefully acknowledge financial support from the Global Frontier Research Program (2011–0032156) funded by the Korean Government (MEST) and Korea Institute of Science and Technology (KIST) internal project (2E23821). C.A.R. acknowledges support of C-SPIN, a STARnet center of DARPA and MARCO, the Semiconductor Research Corp., Tokyo Electron, and TSMC.

Received: May 23, 2014
Revised: July 21, 2014
Published online: September 1, 2014

[1] M. Park, C. Harrison, P. M. Chaikin, R. A. Register, D. H. Adamson, *Science* **1997**, *276*, 1401.
[2] J. Y. Cheng, C. A. Ross, H. I. Smith, E. L. Thomas, *Adv. Mater.* **2006**, *18*, 2505.
[3] M. Lazzari, M. A. López-Quintela, *Adv. Mater.* **2003**, *15*, 1583.
[4] J. Y. Cheng, C. A. Ross, E. L. Thomas, H. I. Smith, G. J. Vancso, *Adv. Mater.* **2003**, *15*, 1599.
[5] E. A. Jackson, M. A. Hillmyer, *ACS Nano* **2010**, *4*, 3548.
[6] J. Yin, X. Yao, J.-Y. Liou, W. Sun, Y.-S. Sun, Y. Wang, *ACS Nano* **2013**, *7*, 9961.
[7] J.-H. Lee, C. Y. Koh, J. P. Singer, S.-J. Jeon, M. Maldovan, O. Stein, E. L. Thomas, *Adv. Mater.* **2014**, *26*, 532.
[8] *International Technology Roadmap for Semiconductors, ITRS 2011 Edition*; 2011.
[9] I. W. Hamley, *The Physics of Block Copolymers*, Oxford University Press, New York **1999**.
[10] E. Sivaniah, Y. Hayashi, S. Matsubara, S. Kiyono, T. Hashimoto, K. Fukunaga, E. J. Kramer, T. Mates, *Macromolecules* **2005**, *38*, 1837.
[11] T. Thurn-Albrecht, J. Schotter, G. A. Kästle, N. Emley, T. Shibauchi, L. Krusin-Elbaum, K. Guarini, C. T. Black, M. T. Tuominen, T. P. Russell, G. A. Kastle, *Science* **2000**, *290*, 2126.
[12] E. Huang, L. Rockford, T. P. Russell, C. J. Hawker, *Nature* **1998**, *395*, 757.
[13] B. H. Sohn, S. H. Yun, *Polymer* **2002**, *43*, 2507.
[14] J. G. Son, X. Bulliard, H. Kang, P. F. Nealey, K. Char, *Adv. Mater.* **2008**, *20*, 3643.
[15] A. M. Welander, H. Kang, K. O. Stuen, H. H. Solak, M. Müller, J. J. de Pablo, P. F. Nealey, *Macromolecules* **2008**, *41*, 2759.
[16] A. P. Smith, A. Sehgal, J. F. Douglas, A. Karim, E. J. Amis, *Macromol. Rapid Commun.* **2003**, *24*, 131.

[17] T. L. Morkved, H. M. Jaeger, *Europhys. Lett.* **1997**, *40*, 643.
[18] M. J. Fasolka, P. Banerjee, A. M. Mayes, G. Pickett, A. C. Balazs, *Macromolecules* **2000**, *33*, 5702.
[19] D. Y. Ryu, J.-Y. Wang, K. A. Lavery, E. Drockenmuller, S. K. Satija, C. J. Hawker, T. P. Russell, *Macromolecules* **2007**, *40*, 4296.
[20] J. G. Son, H. Kang, K.-Y. Kim, J.-S. Lee, P. F. Nealey, K. Char, *Macromolecules* **2012**, *45*, 150.
[21] E. Huang, P. Mansky, T. P. Russell, C. Harrison, P. M. Chaikin, R. a. Register, C. J. Hawker, J. Mays, *Macromolecules* **2000**, *33*, 80.
[22] J. G. Kennemur, L. Yao, F. S. Bates, M. A. Hillmyer, *Macromolecules* **2014**, *47*, 1411.
[23] S. Ji, C.-C. Liu, J. G. Son, K. Gotrik, G. S. W. Craig, P. Gopalan, F. J. Himpsel, K. Char, P. F. Nealey, *Macromolecules* **2008**, *41*, 9098.
[24] C. M. Bates, T. Seshimo, M. J. Maher, W. J. Durand, J. D. Cushen, L. M. Dean, G. Blachut, C. J. Ellison, C. G. Willson, *Science* **2012**, *338*, 775.
[25] M. J. Maher, C. M. Bates, G. Blachut, S. Sirard, J. L. Self, M. C. Carlson, L. M. Dean, J. D. Cushen, W. J. Durand, C. O. Hayes, C. J. Ellison, C. G. Willson, *Chem. Mater.* **2014**, *26*, 1471.
[26] C. M. Bates, M. J. Maher, A. Thio, L. M. Dean, J. D. Cushen, J. Durand, G. Blachut, L. Li, C. J. Ellison, C. G. Willson, *J. Photopolym. Sci. Technol.* **2013**, *26*, 223.
[27] S. H. Kim, M. J. Misner, T. Xu, M. Kimura, T. P. Russell, *Adv. Mater.* **2004**, *16*, 226.
[28] J. Bang, S. H. Kim, E. Drockenmuller, M. J. Misner, T. P. Russell, C. J. Hawker, *J. Am. Chem. Soc.* **2006**, *128*, 7622.
[29] E. M. Freer, L. E. Krupp, W. D. Hinsberg, P. M. Rice, J. L. Hedrick, J. N. Cha, R. D. Miller, H.-C. Kim, *Nano Lett.* **2005**, *5*, 2014.
[30] C. Sinturel, M. Vayer, M. Morris, M. A. Hillmyer, *Macromolecules* **2013**, *46*, 5399.
[31] J. G. Son, J.-B. Chang, K. K. Berggren, C. A. Ross, *Nano Lett.* **2011**, *11*, 5079.
[32] J. G. Son, A. F. Hannon, K. W. Gotrik, A. Alexander-Katz, C. A. Ross, *Adv. Mater.* **2011**, *23*, 634.
[33] Y. S. Jung, J. B. Chang, E. Verploegen, K. K. Berggren, C. A. Ross, *Nano Lett.* **2010**, *10*, 1000.
[34] J. K. W. Yang, Y. S. Jung, J.-B. Chang, R. a Mickiewicz, A. Alexander-Katz, C. A. Ross, K. K. Berggren, *Nat. Nanotechnol.* **2010**, *5*, 256.
[35] S. Wu, in *Polymer Handbook*, (Eds: J. Brandrup, E. H. Immergut, E. A. Grulke, A. Abe, D. R. Bloch), John Wiley & Sons, Hoboken, NJ **2005**, pp. 521–541.
[36] J. G. Son, K. W. Gotrik, C. A. Ross, *ACS Macro Lett.* **2012**, *1*, 1279.
[37] J. M. di Meglio, R. Ober, L. Paz, C. Taupin, P. Pincus, S. Boileau, *J. Phys.* **1983**, *44*, 1035.
[38] S. B. Bahrami, S. S. Kordestani, H. Mirzadeh, P. Mansoori, *Iran. Polym. J.* **2003**, *12*, 139.
[39] D. M. Koenhen, C. A. Smolders, *J. Appl. Polym. Sci.* **1975**, *19*, 1163.
[40] E. A. Grulke, in *Polymer Handbook*, (Eds: J. Brandrup, E. H. Immergut, E. A. Grulke, A. Abe, D. R. Bloch) John Wiley & Sons, Hoboken, NJ **2005**, pp. 675–688.
[41] Y. S. Jung, C. A. Ross, *Adv. Mater.* **2009**, *21*, 2540.
[42] W. A. Phillip, M. A. Hillmyer, E. L. Cussler, *Macromolecules* **2010**, *43*, 7763.
[43] S. P. Paradiso, K. T. Delaney, C. J. Garc, H. D. Ceniceros, G. H. Fredrickson, *ACS Macro Lett.* **2014**, *3*, 16.
[44] M. Y. Paik, J. K. Bosworth, D.-M. Smilges, E. L. Schwartz, X. Andre, C. K. Ober, *Macromolecules* **2010**, *43*, 4253.